

Written by: David Drapcho, Product Manager, Digilab LLC

Fourier Transform infrared (FT-IR) instruments are commonly used in polarization modulation IR measurements. These measurements include linear dichroism (LD) studies for the characterization of monolayer films by reflection absorption and uniaxial deformation of polymer films, and vibrational circular dichroism (VCD) to determine the chiral properties of biological compounds in solution. A common requirement of these measurements is the necessity to demodulate the detector signal for the high frequency polarization modulation-induced differential absorbance. Up to the present, the signal demodulation has been achieved with a lock-in amplifier (LIA) or customized electronic demodulator, adding extra cost and complexity to the experimental system.

We have previously provided the capability of performing signal demodulation on the spectrometer computer using digital signal processing (DSP) software in Resolutions Pro software. These techniques have been applied to the demodulation of step scan phase modulation signals generated by a photo-acoustic detector<sup>1</sup>, and to simultaneous demodulation of phase modulation and a low frequency mechanical strain in dynamic polymer stretching measurements<sup>2</sup>. In this paper we will extend the previous methods to demodulation of the high frequency signal generated by the photoelastic modulator (PEM) in infrared reflection absorption (IRRAS) measurements of self-assembled monolayers.

## Experimental

A schematic diagram of an IRRAS experiment is shown in Figure 1. Broad band infrared radiation from a ceramic source is phase modulated by a Varian FTS 7000 step scan interferometer, typically at phase modulation frequencies of 400 or 800 Hz at an amplitude of 1.0 or 2.0  $\lambda$  HeNe, and stepping at 0.5-2.5 Hz. The modulated radiation is filtered with a lowpass optical filter transmitting radiation below 3950  $\text{cm}^{-1}$  or 1975  $\text{cm}^{-1}$ . The IR light is filtered to undersample the interferogram by 4 or 8, thereby reducing the measurement time. After filtering, the IR radiation is polarized by a gold grid polarizer, then polarization modulated by a Hinds ZnSe PEM operating at 37 KHz and amplitude of 0.5  $\lambda$  (strain axis 45° to the polarizer), before reflecting off the sample at grazing angle of incidence; 80° to 85° from normal. The sample is a self-assembled monolayer film on a metallic substrate, typically gold. The IR light is subsequently focused onto a narrow band MCT detector with on-axis refractive optics. The spectrometer step and phase modulation are controlled by the master clock on the spectrometer. The PEM operates asynchronously with the spectrometer.

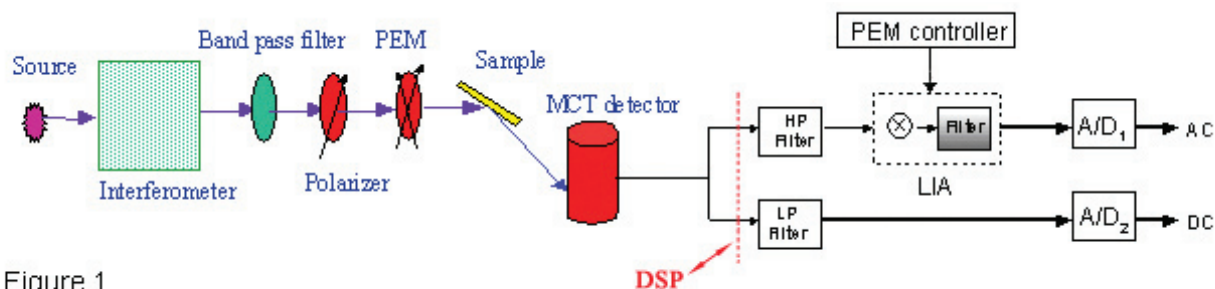


Figure 1

After the detector and preamplifier, the demodulation method as first described by Marcott<sup>3</sup> is displayed in the figure above. This method employs a set of electronic filters and a lock-in amplifier (LIA) along two parallel signal paths. In the top path above, the detector signal is high-pass filtered, then demodulated for polarization modulation by a lock-in amplifier (LIA). The output of the LIA provides the dichroic difference spectrum between s and p polarized light, often called the AC spectrum. Since the electric field of s-polarized light has a node at the surface of a metallic substrate, only absorption of p-polarized light can be observed from the monolayer coating, and the dichroic difference spectrum,  $R_p - R_s$ , is the only polarization sensitive component in the optical path. Thus the upper signal path is sensitive only to the thin film on the substrate, allowing the surface signal to be digitized with high dynamic range, enhancing the sensitivity for analysis of such samples. In the lower path above, the detector is low-pass filtered to eliminate the high frequency PEM component, providing the single beam spectrum of the substrate. The final step of data processing is to ratio the AC to the DC spectrum providing the surface spectrum with high sensitivity and free from atmospheric contamination and other artifacts. The latter statement is true if the AC and DC channels are sampled simultaneously with parallel A/D converters. As shown by the red dashed box, the digital signal processing (DSP) software described below will replace the function of the LIA, the electronic filters and second A/D converter.

## DSP Algorithm

Before discussing the DSP algorithm, we must first understand the signals generated in a PEM-IRRAS measurement for polarization modulation at 37 KHz (detected at 74 KHz) and phase modulation (PM) at 400 Hz. A schematic spectrum of the signals is shown in Figure 2. The 74 KHz linear dichroism frequency (LD) acts as a carrier for the lower frequency signals, with PM sidebands at  $\pm 400$  Hz around the PEM carrier. An examination of this spectrum shows that there is a large gap in the spectrum between the PM frequency and the PEM frequency (approximately between 1 KHz and 70 KHz) where there is no useful information. With this knowledge, we can design a simple electronic filter, as shown in the top part of the Figure 3 below, with a bandpass below 2 KHz and a bandpass  $\pm 4$  KHz around 74 KHz. Such a filter will allow undersampling the detector signal with the spectrometer A/D converter, thereby reducing the size of the data array. Sampling the 74 KHz signal with minimal Nyquist sampling criterion would require an A/D rate  $\sim 150$  KHz. Such a sampling rate would generate data files on the order of hundreds of Mb for all interferogram retardation points. Since the data will require  $\sim N^k$  (with  $k > 1$ ) operations, we wish to reduce the numbers of samples,  $N$ , to be processed.

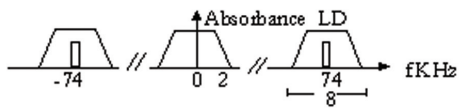


Figure 3

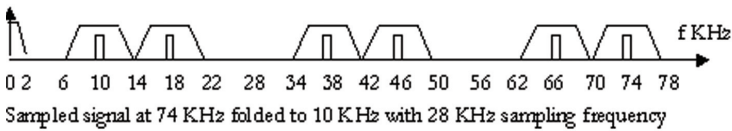
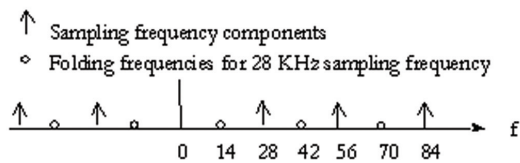


Figure 3 shows the effect of sampling the detector signal at 28 KHz with an anti-aliasing filter as shown on the top. An A/D rate of 28 KHz will produce folding points at 14 KHz and at 28 KHz intervals thereafter. Signals near 74 KHz will fold to 10 KHz, and replicas of this signal will appear at 18 KHz, 38 KHz, 46 KHz, etc. Undersampling with the anti-alias filter reduces the size of the data array by approximately 5 times without sacrificing sensitivity.

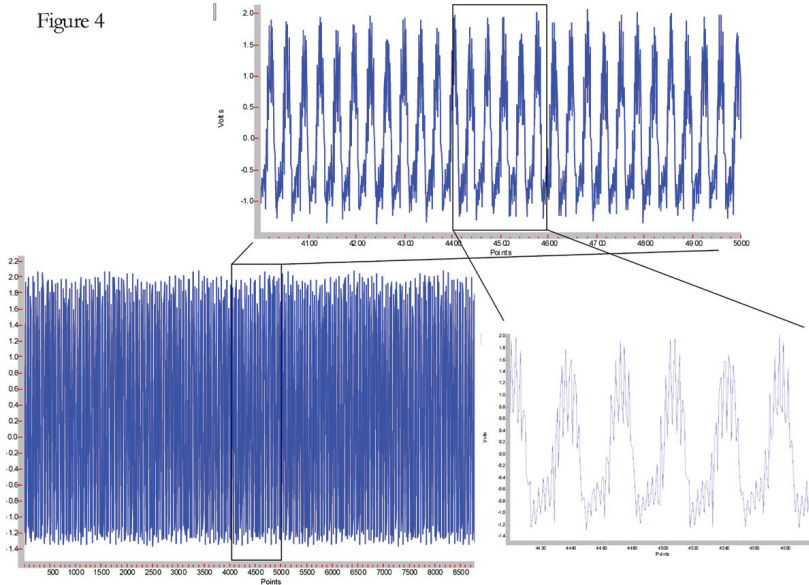


Figure 4

As an example, PEM-IRRAS data were collected in the time domain at each step of the interferogram at a step rate of 2.5 Hz, PM frequency of 800 Hz with an amplitude of  $1.0 \lambda$ , and PEM operating with  $0.5 \lambda$  retardation at a frequency of 36966 Hz (73932 2nd harmonic). A portion of the raw data collected at a step near the centerburst is displayed in Figure 4, with the insets showing expansions of the data. The undersampled PEM signal (higher frequency fluctuation) and PM signal (distorted square wave) can be recognized in the lower right inset. A Fourier transform of the time domain data generates the frequency magnitude spectrum displayed in the lower panel of Figure 5, showing the phase modulation frequency at 800 Hz and its odd harmonics (resulting from square wave phase modulation), and the second harmonic of the PEM frequency which folds to 9362 Hz when sampled at 27.778 KHz.

Figure 5 shows the effect of sampling the detector signal at 28 KHz with an anti-aliasing filter as shown on the top. An A/D rate of 28 KHz will produce folding points at 14 KHz and at 28 KHz intervals thereafter. Signals near 74 KHz will fold to 10 KHz, and replicas of this signal will appear at 18 KHz, 38 KHz, 46 KHz, etc. Undersampling with the anti-alias filter reduces the size of the data array by approximately 5 times without sacrificing sensitivity.

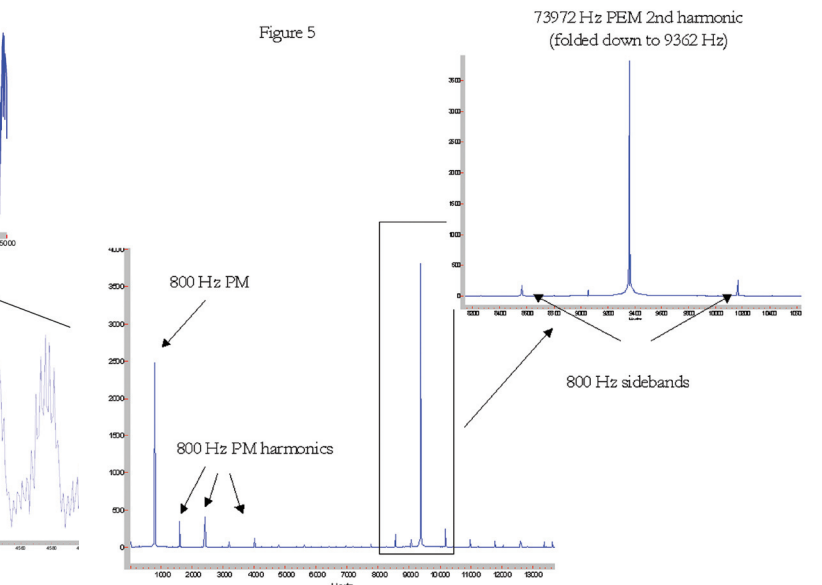


Figure 5

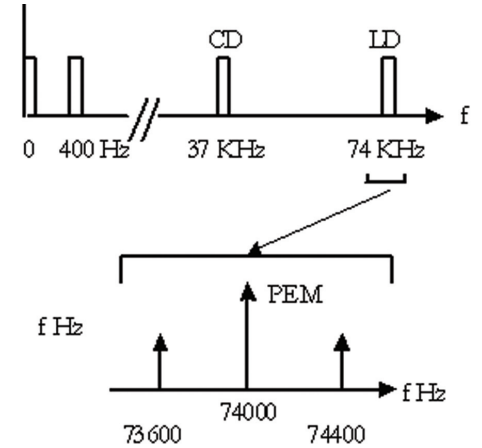


Figure 2

The region around the PEM frequency is expanded in the upper panel, showing the 800 Hz PM sidebands. The PEM operates asynchronously with the spectrometer, and its frequency and phase must be measured with high precision<sup>4</sup>. We select three sets of  $M$  samples out of the  $N$  total samples in the first step of the interferogram, as shown in Figure 6, and apodize each set with a triangular window. First, we determine the phase error in the middle of interval I with respect to an initial estimate for the PEM frequency,  $\omega_0$ .

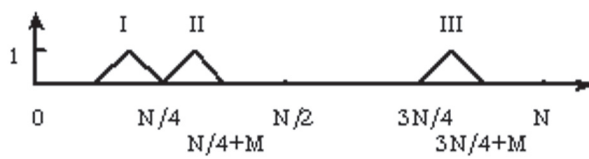
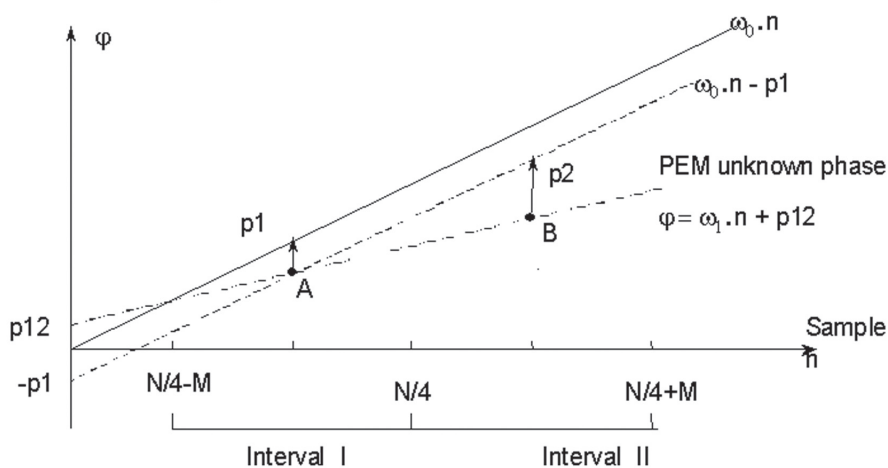


Figure 6

$$p1 = \arg \left[ \sum_{N/4-M}^{N/4} x_n e^{i\omega_0 n} \right]$$

The phase of the PEM signal as a function of sample point (time) is displayed in Figure 7, showing how the actual frequency,  $\omega_M$  (the slope of the dash-dot line) will be different from the initial estimate,  $\omega_0$  (the slope of the solid line). After correcting the phase of  $\omega_0$  for  $p1$  (dashed line), the phase of  $\omega_0$  and  $\omega_M$  intersect at point A below. With the phase error  $p1$ , we can compute the error  $p2$  in interval II,

Figure 7



$$p2 = \arg \left[ \sum_{N/4}^{N/4+M} x_n e^{i(\omega_0 n - p1)} \right]$$

which then allows a refinement of the PEM frequency,

$$\omega_1 = \omega_0 - \frac{p2}{M}$$

to provide the phase error  $p12$  for  $\omega_1$ . 
$$p12 = \arg \left[ \sum (\omega_0 - \omega_1) \left( \frac{N}{4} - \frac{M}{2} \right) - p1 \right]$$

With  $p12$ , we compute the phase error,  $p3$ , for  $\omega_1$  in interval III, 
$$p3 = \arg \left[ \sum_{3N/4}^{3N/4+M} x_n e^{i(\omega_1 n + p12)} \right]$$

leading to the final refinement of the PEM frequency in interval III,  $\omega_3$ . 
$$\omega_3 = \omega_1 - \frac{p3}{\left( \frac{N}{2} + M \right)}$$

A separate calibration step<sup>2,4</sup> is required prior to sample analysis to calibrate for the phase of the phase modulation frequency relative to the spectrometer clock. This calibration is performed with the monolayer sample itself, no other calibration sample is required. After calibration, the phase parameters are stored in the data system and the sample response to the simultaneous modulations can be computed as:

- Static Absorbance (DC)

$$SA(m) = \sum_n x(n,m) \cdot \cos(\omega_\phi t - \theta_\phi)$$

- In-phase Polarization Modulation (AC)

$$PEM_I(m) = \sum_n x(n,m) \cdot \cos(\omega_\phi t - \theta_\phi)$$

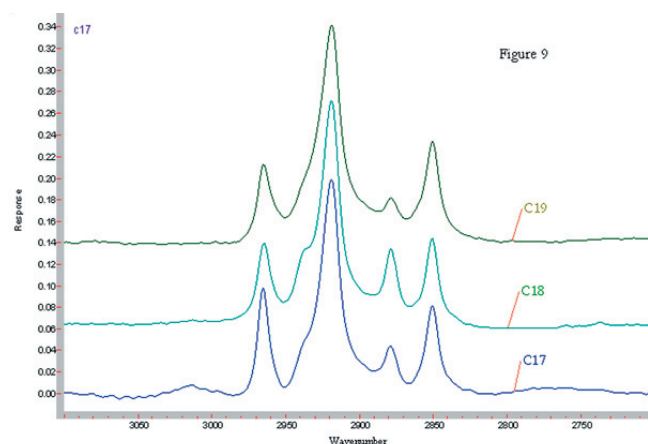
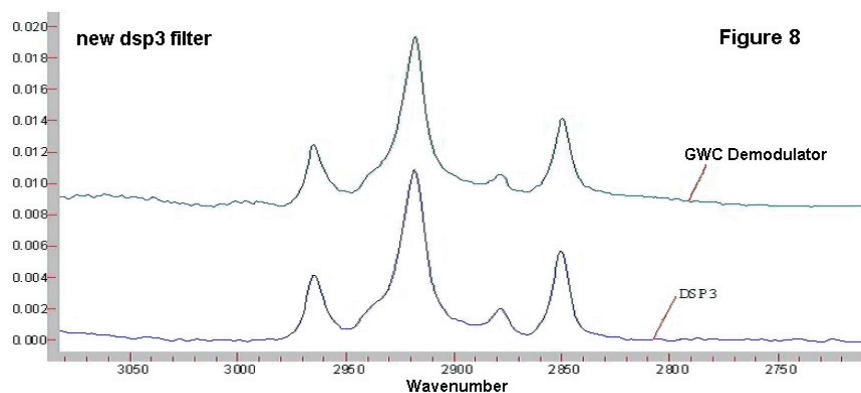
- In-phase PEM Phase Modulation sideband (AC)

$$PEM - PM_I(m) = \sum_n x(n,m) \cdot \cos(\omega_\phi t - \theta_\phi) \cos(\omega_\phi t - \theta_\phi)$$

## Results

A self-assembled monolayer of a long chain alkane thiol on gold was used as a test sample to test the performance of the DSP software versus the conventional processing method as shown in Figure 1. The demodulator used in this measurement was a GWC SSD-74 demodulator optimized for a 37 KHz ZnSe PEM.

The GWC data was collected in rapid scan mode at 20 KHz scan speed, with a measurement time of approximately 20 minutes to be consistent with the DSP measurement time. The results of the two methods are displayed in Figure 8, expanding the spectra around the C-H stretching region, with the rapid scan results collected with the GWC demodulator on the top, and the DSP results on the bottom. All spectra were processed by ratioing the AC spectrum to the DC spectrum, as described above, then baseline correcting to remove the polarization modulation efficiency Bessel function profile.



An examination of the spectra shows the performance to be approximately equivalent between the two methods, with perhaps a small advantage to the DSP method. A series of alkane-thiol self-assembled monolayer films, with carbon chain lengths from 17 to 19 carbon atoms, were prepared on gold substrates. DSP spectra collected of these samples are displayed in Figure 9, again expanded around the C-H stretching region. Examination of Figure 9 shows the characteristic dependence in the intensity ratio of methyl to methylene CH to even or odd carbon chain length.

## Conclusions

DSP software has been shown to be a suitable replacement for a LIA for demodulation of the high frequency signals in grazing angle PEM-IRRAS experiments. Results with DSP are equivalent or superior to those obtained with a LIA, with the additional benefit of eliminating the cost and experimental complexity of the external electronics and second digitizer channel.

## References

- <sup>1</sup>D.L. Drapcho, R. Curbelo, E.Y. Jiang, R.A. Crocombe, and W.J. McCarthy, Applied Spectroscopy, 51, 453 (1997) and US Patent 5,612,784
- <sup>2</sup>US Patents 5,835,213 and 6,020,962
- <sup>3</sup>C. Marcott, Applied Spectroscopy, 38, 442 (1984)
- <sup>4</sup>R. Curbelo, AIP Conference Proceedings 430, 74 (1998); and US Patent 6,025,913



**VARIAN**

Varian, Inc. • [www.varianinc.com](http://www.varianinc.com)

- North America 1.800.926.3000, 1.925.939.2400
- Europe The Netherlands 31.118.67.1000
- Asia Pacific Australia 613.9560.7133
- Latin America Brazil 55.11.3845.0444

- China 86.21.6375.6969
- Japan 81.3.5232.1239
- Korea 82.2.3452.2452
- Taiwan 886.22.698.9555
- Other sales offices and dealers throughout the world

GC • LC • MS • AAS • ICP • UV-Vis-NIR • FT-IR • Raman • Fluorescence • Dissolution • NMR • Consumable Products